Journal of Materials Chemistry A

Accepted Manuscript

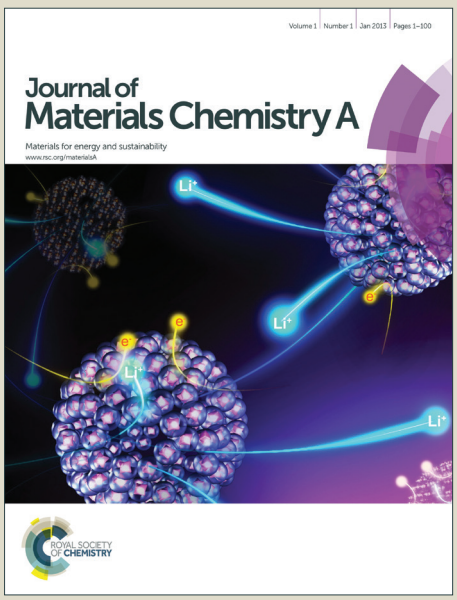

ROYAL SOCIETY OF CHEMISTRY

www.rsc.org/materialsA

$ZnCo_2O_4$ nanowire arrays grown on nickel foam for high-performance psuedocapacitors

Shubo Wang, Jun Pu, Yao Tong, Yuanyuan Cheng, Yan Gao, Zhenghua Wang*

Key Laboratory of Functional Molecular Solids, Ministry of Education, College of Chemistry and Materials Science, Anhui Normal University, Wuhu 241000, P. R. China

*Corresponding author. Tel.: +86-553-3869303; Fax: +86-553-3869302; E-mail: zhwang@mail.ahnu.edu.cn.

Abstract

Uniform $ZnCo_2O_4$ nanowire arrays were directly grown on nickel foam through a facile hydrothermal method and subsequent thermal treatment process. The $ZnCo_2O_4$ nanowires have diameters of about 100 nm and lengths of up to 5 μm. The as-obtained $ZnCo_2O_4$ nanowire arrays loaded nickel foam can be directly applied as electrode for high-performance supercapacitors. Electrochemical measurements show that the $ZnCo_2O_4$/nickel foam electrode has high specific capacitance (1625 F g^{-1} at 5 A g^{-1}), excellent rate capability (59% capacitance retention at 80 A g^{-1}) and good cycling stability (94% capacitance retention over 5000 charge–discharge cycles). This work demonstrates that $ZnCo_2O_4$ nanowires are highly desirable in the application of advanced elecrochemical electrode materials.

1. Introduction

The demands for high-performance, lightweight, and environmentally friendly energy storage devices have been greatly increased with the rapid development of modern electronic industry. [1–3] Supercapacitors, also called electrochemical capacitors, have attracted great attentions due to their high power density, fast charge/discharge rates, long cycle lifetime and low cost as comparing to rechargeable batteries, and have shown great perspects in areas of uninterruptible power supplies, hybrid electrical vehicle systems, aerospace, emergency lighting, and renewable energies.[4–7]

In general, supercapacitors can be classified into electric double layer capacitors (EDLCs) and pseudocapacitors on the basis of the charge storage mode.[8,9] The capacitance of EDLCs relies on charge separation at the interface of electrolyte and electrodes. Carbon-based materials such as activated carbon, carbon nanocages and graphene have been widely used as electrodes for EDLCs due to their high specific-area, good electrical conductivity, long cycle life and low cost.[10–12] However, their specific capacitance is still limited. On the contrary, pseudocapacitors arising from fast reversible faradic process of redox-active materials can provide much higher specific capacitances than EDLCs. Many transition metal oxides, such as NiO, SnO_2, Co_3O_4 and Mn_3O_4 have been extensively studied as possible electrode materials for pseudocapacitors.[13–16] However, their slow ion diffusion rates and poor electron conductivity would inhibit their applications as high-performance supercapacitors electrodes with high rate capability.

Recently, the growth of electrode materials directly on conductive substrates as supercapacitors electrode has attracted more and more attentions. Such a binder-free method can improve the interfacial contact between the current collector and the active materials and enhance ion transportation, therefore, the electrochemical performances of supercapacitors can be greatly improved. $Co(OH)_2$, and $NiCo_2O_4$ have been directly grown on various conductive substrates including copper substrate, carbon fiber paper, stainless-steel foil, titanium foil and nickel foam,[7,17–20] and have revealed better pseudocapacitive performances.

Recent studies have shown that binary metal oxides such as $NiCo_2O_4$ can exhibit better electrochemical performance than single-component metal oxides due to their electron conductivity and richer redox reactions.[21–23] $ZnCo_2O_4$ with spinel structure has been investigated for applications in areas of Li-ion batteries, electrocatalysts, gas sensors, etc.[24–27] However, reports on $ZnCo_2O_4$ materials as electrodes for supercapacitors are still limited.[28,29] Very recently, Shen et al. reported $ZnCo_2O_4$ nanorods/nickel foam architectures prepared through a polyol refluxing process followed by thermal treatment with good capacitive behavior.[30] Herein, we report a simple hydrothermal process followed by thermal treatment method for the direct growth of $ZnCo_2O_4$ nanowire arrays on nickel foam, and the $ZnCo_2O_4$ nanowire arrays loaded nickel foam can be directly used as supercapacitors electrode. The $ZnCo_2O_4$ nanowires are thinner than that prepared by Shen et al, which may be more favorable for the inward diffusion of electrolyte ions. Electrochemical tests show that the $ZnCo_2O_4$ nanowire/nickel foam electrode has a better electrochemical

performance, with a higher specific capacitance of 1625 F g^{-1} at 5 A g^{-1} and an excellent rate capacity (59% capacity retention at 80 A g^{-1}). Furthermore, a capacitance retention of 94% after 5000 charge–discharge cycles at 20 A g^{-1} is obtained, indicating excellent cycling stability of the $ZnCo_2O_4$ nanowires/nickel foam electrode.

2. Experimental details

2.1 Materials

Zinc nitrate hexahydrate ($Zn(NO_3)_2·6H_2O$), cobalt nitrate hexahydrate ($Co(NO_3)_2·6H_2O$), urea ($CO(NH_2)_2$), ammonium fluoride (NH_4F), hydrochloric acid (HCl), potassium hydroide (KOH), absolute ethanol, all these reagents were purchased from Sinopharm Chemical Reagent Co., Ltd. with analytical grade. Deionized water was used throughout.

2.2 Synthesis of $ZnCo_2O_4$ nanowire arrays

In a typical procedure, $Zn(NO_3)_2·6H_2O$ (1 mmol, 0.297 g), $Co(NO_3)_2·6H_2O$ (2 mmol, 0.582 g), $CO(NH_2)_2$ (5 mmol, 0.300 g) and NH_4F (2 mmol, 0.074 g) were together added into 40 mL deionized water under stirring to form a red solution. A piece of nickel foam (1 cm × 1 cm) was treated with 6 M HCl for 10 min to remove the oxide layer and then washed thoroughly with deionized water. The mixed solution and the nickel foam were together transferred into Teflon-lined stainless-steel autoclave with a capacity of 50 mL, heated in an oven at 120 °C for 5 h, and then allowed to cool to room temperature naturally. The nickel foam coated with precursor

was rinsed with deionized water, dried in vacuum at 50 °C for 2 h, and then heated under ambient atmosphere at 400 °C for 2 h.

The mass of $ZnCo_2O_4$ nanowire arrays on nickel foam is 0.6 mg by weighing the nickel foam before and after the loading of $ZnCo_2O_4$, and the estimated loading of active material is about 0.6 mg cm^{-2}.

2.3 Characterizations

X-ray powder diffraction (XRD) patterns were obtained on a Rigaku Max-2200 X-ray diffractometer with Cu Kα radiation (λ = 0.15406 nm) in the 2θ range of 20–80°. X-ray photoelectron spectroscopy (XPS) were recordered on an ESCALab MKII X-ray photoelectron spectrometer with nonmonochromatized Mg-Kα X-ray as the excitation source. The binding energies in XPS analysis were corrected by referencing C1s to 284.6 eV. The field emission scanning electron microscopy (FESEM) images were taken with a Hitachi S-4800 scanning electron microscope. Transmission electron microscopy (TEM) images, high-resolution transmission electron microscopy (HRTEM) images and energy dispersive X-ray spectrum (EDX) were recorded on a FEI Tecnai G^2 20 high-resolution transmission electron microscope equipped with an energy dispersive X-ray analysis system. Electrochemical measurements were carried out on an electrochemical working station (CHI660D).

2.4 Electrochemical measurements

A three electrode experimental setup was applied to examine the electrochemical activities of the prepared sample. The $ZnCo_2O_4$ nanowire arrays loaded nickel foam

(1.0 cm × 1.0 cm) directly acted as the working electrode, platinum wire and saturated calomel electrode (SCE) acted as the counter and reference electrodes, respectively. A 3 M KOH aqueous solution was used as the electrolyte.

The specific capacitance (C) of the electrode can be evaluated according to the following equation.[31,32]

$$C = \frac{I \times \Delta t}{m \times \Delta V} \quad (1)$$

where C (F g^{-1}) is the specific capacitance of the electrode based on the mass of active materials, I (A) is the current during discharge process, Δt (s) is the discharge time, ΔV (V) is the potential window (here ΔV = 0.45 V), m (g) is the mass of active materials.

The electrochemical performances of the $ZnCo_2O_4$ nanowire arrays/nickel foam electrode was also measured using a two-electrode experimental setup. The $ZnCo_2O_4$ nanowire arrays loaded nickel foam (1.0 cm × 1.0 cm) directly acted as the electrode. Two symmetry electrodes were immersed into a beaker containing 3 M KOH solution with a distance of 15 mm between the centers.

The specific capacitances, energy density (E) and power density (P) derived from galvanostatic tests can be calculated according to the following equations[12,33]:

$$C = 4 \times \frac{I \times \Delta t}{m \times \Delta V} \quad (2)$$

$$E = \frac{1}{8} C \Delta V^2 \quad (3)$$

$$P = \frac{E}{\Delta t} \quad (4)$$

3. Results and discussion

The formation process of $ZnCo_2O_4$ nanowire arrays on nickel foam were illustrated in Fig. 1. The fabrication include two steps. Firstly, the raw materials reacted under hydrothermal conditions and formed precursor nanowire arrays aligned on nickel foam. The nickel foam change from gray to light blue due to the coating of the precursor on nickel foam. Next, the precursor coated nickel foam was calcined in air. A color change from light blue to black indicating the transformation from the precursor nanowires to $ZnCo_2O_4$ nanowires. Finally, the nickel foam supported $ZnCo_2O_4$ nanowire arrays were obtained. As the $ZnCo_2O_4$ nanowires were directly grown on nickel foam, the high-quality contact between the active materials and the current collector is highly desirable to reduce the contact resistance and lead to high capacitive performances.

Fig. 2a depicts a SEM image of the pristine nickel foam with three-dimensional network structure and smooth surfaces. After the first step hydrothermal reaction at 120 °C for 5 h, high-density precursor nanowires were found deposited on the whole nickel foam, as indicated from the inset in Fig. 2b. Magnified SEM images of the precursor shown in Fig. 2b clearly reveals that the as-obtained precursor nanowires are straight and thin, and are uniform in size, with an average diameter of about 100 nm and lengths up to 5 μm. Fig. 2c displays a SEM image of the $ZnCo_2O_4$ sample obtained by calcining the precursor in air at 400 °C for 2 h, which shows almost the same feature as that of the precursor. Magnified view of the $ZnCo_2O_4$ sample in Fig. 2d reveals that the $ZnCo_2O_4$ nanowires are porous. The porous structure of the

$ZnCo_2O_4$ nanowires is formed due to the release of gaseous species during the calcining process.

A typical XRD pattern of the $ZnCo_2O_4$ sample is shown in Fig. 3a. To avoid the affection of nickel foam, the $ZnCo_2O_4$ sample was separated from the nickel foam through long time ultrasonication. All of the diffraction peaks in this pattern can be readily indexed to face-centered cubic $ZnCo_2O_4$ (JCPDS card No. 23-1390). The broad diffraction peaks indicating the tiny size of the $ZnCo_2O_4$ sample. EDX spectrum of the $ZnCo_2O_4$ nanowires is shown in Fig. 3b. Zn and Co elments together with O elements are present, consistent with the the composition of $ZnCo_2O_4$. C element is come from the carbon paste. No other redundant element can be found in this spectrum. Fig. 3c shows a TEM image of a $ZnCo_2O_4$ nanowire, which clearly indicates the porous structure of the $ZnCo_2O_4$ nanowire. Fig. 3d demonstrates a HRTEM image of the porous $ZnCo_2O_4$ nanowire. The observed interplanar spacing is 0.23 and 0.24 nm, corresponding to the separation between (222) and (311) lattice planes of $ZnCo_2O_4$.

The chemical bonding states of each element on the surface of $ZnCo_2O_4$ nanowires are evaluated by XPS technique. The XPS survey spectrum shown in Fig. 4a indicates the presence of Co, Zn and O elements. The C elements is due to exposure to the air. The core level spectrum of the Co 2p region is shown in Fi.g 4b, the stong peaks at 795.2 eV for Co 2 $p_{3/2}$ and 780.0 eV for Co $2p_{1/2}$ are demonstrated, indicating the Co^{3+} oxidation state of the $ZnCo_2O_4$ sample.[34,35] Fig. 4c shows the core level spectrum of Zn 2p region. The stong peaks at 1045.7 and 1022.5 eV correspond to Zn $2p_{3/2}$ and Zn

$2p_{1/2}$ of Zn (II), respectively.[36] In the O 1s spectrum (Fig. 4d), three peaks at 529.5, 531.1 and 532.1 eV well consistent with the reported values.[22]

The capacitive performance of the as-obtained $ZnCo_2O_4$ nanowires/nickel foam electrode was evaluated by cycle voltammetry (CV) and galvanostatic charge–discharge measurements in a 3 M KOH aqueous solution using a three electrode system at room temperature. Fig. 5a demonstrates the CV curves of the $ZnCo_2O_4$ nanowire arrays on nickel foam directly applied as electrode at various scan rates ranging from 5 to 100 mV s^{-1} in a potential range of −0.1 to 0.4 V versus Ag/AgCl. The shapes of the present CV curves are distinctly different from the CV curves of EDLCs that are close to an ideal rectangular shape. Clearly, a pair of redox peaks is visible in the CV curves, indicating that the electrochemical performance of the $ZnCo_2O_4$ nanowires is result from the pseudocapacitive capacitance. At a scan rate of 5 mV s^{-1}, the CV curve exhibit a shoulder peak at around 0.27 V, and corresponding cathodic peak at about 0.16 V. In addition, it can be seen that the redox peaks positions progressively shifts with the increase of the scan rate, which can be explained by the diffusion of OH^- ions into the $ZnCo_2O_4$ nanowires. At different scan rates, the movement speed of OH^- ions is different, and the utilization ratio of electrode active material is different, too.[37] The redox peaks can be assigned to the $Co(OH)_2$/CoOOH redox couple prior to the onset of oxygen evolution, illustrating high redox reversibility of these electrodes.[30]

As nickel foam can be oxidized during annealing, and nickel oxide can also contribute to capacitance, we have tested the annealed nickel foam using CV, and the

CV curves of annealed nickel foam and $ZnCo_2O_4$ nanowire arrays loaded nickel foam at 100 mV s^{-1} are shown in Fig. 5b. It is observed that the CV curve of annealed nickel foam is almost a straight line, revealing that nickel foam is not seriously oxidized during the annealing process, and the electrochemical performance of as-obtained $ZnCo_2O_4$ nanowires/nickel foam electrode is completely come from $ZnCo_2O_4$ nanowires.

Galvanostatic charge–discharge curves of the $ZnCo_2O_4$ nanowire arrays loaded nickel foam electrode at different current densities in the potential window of −0.1–0.4 V are shown in Fig. 5c. All of the curves are symmetric in shape during the charge–discharge process, indicative of fairly good pseudocapacitive behaviors. On the basis of the discharging times, a series of specific capacitances against various current densities are obtained from formula (1), as shown in Fig. 5d. The specific capacitances are about 1625, 1536, 1444, 1182 and 962 F g^{-1} at current densities of 5, 10, 20, 40 and 80 A g^{-1}, respectively. The corresponding areal capacitances are 975, 922, 866, 709 and 577 mF cm^{-2} at 3, 6, 12, 24 and 48 mA cm^{-2}, respectively. At a high density of 80 A g^{-1}, the specific capacitance of the electrode remains at 962 F g^{-1}, 59% of that at 5 A g^{-1}, highlighting the excellent rate capability of the $ZnCo_2O_4$-based electrodes.

Further, the capacitance performance of the $ZnCo_2O_4$ nanowire arrays loaded nickel foam electrode was also evaluated by a two-electrode system for reference. Fig. 6a depicts the CV curves at scan rates of 10–100 mV s^{-1}. Different from the CV curves obtained in three-electrode system, here the CV curves show rectangular-like shape,

revealing the electrode stores electrochemical charge in the way of electrical double-layer.[28] It can also be seen that increasing the scan rates leads to further augmentation of the CV curves, in agreement with the trend revealed by the three-electrode system. Galvanostatic charge–discharge measurements designated at different current densities were conducted and the resultant profiles are given in Fig. 6b. The specific capacitances are obtained from formula (2). According the results, a high specific capacitance of ca. 568 F g^{-1} (341 mF cm^{-2}) can be achieved at a low current density of 2 A g^{-1} (1.2 mA cm^{-2}) and ca. 188 F g^{-1} (113 mF cm^{-2}) at a high current density of 16 A g^{-1} (9.6 mA cm^{-2}). The energy density and power density are obtained from formula (3) and (4). Figu. 6c shows the Ragone plot concerning energy *vs*. Power density. In the case of a low power density of 0.8 kW kg^{-1}, a high energy density of 12.5 Wh kg^{-1} can be obtained. While increasing the power density up to 6.4 kW kg^{-1}, the energy density decreases to be 3.8 Wh kg^{-1} accordingly.

Cycling stability is a major factor that determines the practical applications of supercapacitors electrode materials. Fig. 7a shows the cycling performance of the $ZnCo_2O_4$ nanowires based electrode at a current density of 20 A g^{-1} in the three-electrode system. As seen from this figure, the specific capacitance retention ratio of $ZnCo_2O_4$ nanowire arrays is 94% after 5000 charge–discharge cycles, which shows excellent cycling stability. Electrochemical impedance response of the nickel foam supported $ZnCo_2O_4$ nanowire arrays in the frequency range of 100 kHz to 0.01 Hz is measured, as shown in Fig. 7b. Clearly, the Nyquist plots are composed of a depressed semicircle in the high frequency region and a straight line in the low

frequency, which is characteristic of capacitive behavior and representative of ion diffusion in the electrode.[38] The impedance spectra of the 1st and 100th cycles are very similar, indicating that the $ZnCo_2O_4$ nanowire arrays are suitable for supercapacitors.

The high specific capacity, excellent rate capability, and good cycling stability of the $ZnCo_2O_4$ nanowires-based electrodes may be attributed to the following aspects. Firstly, the 3D structure of nickel foam not only provides more sites for the adsorption of ions, but also facilitate the contact of electrolyts with $ZnCo_2O_4$ nanowires.[39,40] Secondly, the porous structure of $ZnCo_2O_4$ nanowires is advantageous for providing efficient pathways for charge transportation, which could enhance the capacity performance. Finally, the intimate contact between $ZnCo_2O_4$ nanowires and nickel foam ensures excellent conductivity. These factors make the as-obtained nickel foam supported $ZnCo_2O_4$ nanowire arrays promising for high-performance supercapacitors.

4. Conclusions

In summary, nickel foam supported $ZnCo_2O_4$ nanowire arrays are successfully prepared through a facile hydrothermal method and subsequent thermal treatment process. Owing to the porous nanostructure of $ZnCo_2O_4$ nanowires, the 3D structure of nickel foam and the good contact of $ZnCo_2O_4$ nanowires with nickel foam, the $ZnCo_2O_4$ nanowire arrays show an excellent electrochemical performance. The $ZnCo_2O_4$ nanowires/nickel foam electrode exhibits a high specific capacitanceof 1625 F g^{-1} at 5 A g^{-1}. Furthermore, the retention of capacitance is 94% after 5000 cycles at

a high current density of 20 A g^{-1}. The excellent electrochemical performance enables the $ZnCo_2O_4$ nanowire arrays a promising electrode material for the next-generation energy storage device.

Acknowledgements

Financial support from the National Natural Science Foundation of China (Project No. 21171006) is gratefully acknowledged.

References

1 L. L. Zhang and X. S. Zhao, Chem. Soc. Rev., 2009, 38, 2520.

2 T. Chen, L. Qiu, Z. Yang, Z. Cai, J. Ren, H. Li, H. Lin, X. Sun and H. Peng, Angew. Chem. Int. Ed., 2012, 51, 11977.

3 L. F. Chen, Z. H. Huang, H. W. Liang, W. T. Yao, W. T. Yao and S. H. Yu, Energy Environ. Sci., 2013, 6, 3331.

4 L. F. Chen, Z. H. Huang, H. W. Liang, Q. F. Guan and S. H. Yu, Adv. Mater., 2013, 25, 4746.

5 S. Boukhalfa, K. Evanoff and G. Yushin, Energy Environ. Sci., 2012, 5, 6872.

6 D. Q. Liu, Q. Wang, L. Qiao, F. Li, D. S. Wang, Z. B. Yang and D. Y. He, J. Mater. Chem., 2012, 22, 483.

7 G. Q. Zhang and X. W. Lou, Adv. Mater., 2013, 25, 976.

8 P. Simon and Y. Gogotsi, Nat. Mater., 2008, 7, 845.

9 Y. Q. Wu, X. Y. Chen, P. T. Ji and Q. Q. Zhou, Electrochim. Acta., 2011, 56,

7517.

10 Q. Q. Zhou, X. Y. Chen and B. Wang, Micropor. Mesopor. Mater., 2012, 158, 155.

11 Z. J. Fan, Q. K. Zhao, T. Y. Li, J. Yan, Y. M. Ren, J. Feng and T. Wei, Carbon, 2012, 50, 1699.

12 K. Xie, X. Qin, X. Wang, Y. Wang, H. Tao, Q. Wu, L. Yang and Z. Hu, Adv. Mater., 2012, 24, 347.

13 J. W. Lang, L. B. Kong, W. J. Wu, Y.C. Luo and L. Kang, Chem. Commun., 2008, 35, 4213.

14 R. K. Selvan, I. Perelshtein, N. Perkas and A. Gedanken, J. Phys. Chem. C, 2008, 112, 1825.

15 B. Wang, T. Zhu, H. B. Wu, R. Xu, J. S. Chen and X. W. Lou, Nanoscale, 2012, 4, 2145.

16 M. Fang, X. L. Tan, M. Liu, S. H. Kang, X. Y. Hu and L. D. Zhang, CrystEngComm, 2011, 13, 4915.

17 L. Huang, D. C. Chen, Y. Ding, S. Feng, Z. L. Wang and M. L. Liu. Nano Lett., 2013, 13, 3135.

18 J. Liu, C. P. Liu, Y. L. Wan, W. Liu, Z. S. Ma, S. M. Ji, J. B. Wang, Y. C. Zhou, P. Hodgson and Y. C. Li, CrystEngComm, 2013, 15, 1578.

19 G. Q. Zhang, H. B. Wu, H. E. Hoster, B. C. P. Mary and X. W. Lou, Energy Environ. Sci., 2012, 5, 9453.

20 A.D. Jagadale, V.S. Kumbhar, D.S. Dhawale and C.D. Lokhande, Electrochim.

Acta., 2013, 98, 32.

21 C. Z. Yuan, J. Y. Li, L. R. Hou, X. G. Zhang, L. F. Shen and X. W. Lou, Adv. Funct. Mater., 2012, 22 , 4592.

22 J. Pu, J. Wang, X. Q. Jin, F. L. Cui, E. H. Sheng and Z. H. Wang, Electrochim. Acta, 2013, 106, 226.

23 J. Pu, X. Q Jin, J. Wang, F. L. Cui, S. B. Chu, E. H. Sheng and Z. H. Wang, J. Electroanal. Chem. 2013, 707, 66.

24 B. Liu, X. F. Wang, B. Y. Liu, Q. F. Wang, D. S. Tan, W. F. Song, X. J. Hou, D. Chen and G. Z. Shen, Nano. Res., 2013, 6, 525.

25 C. Lin, Y. Y. Li, M. Yu, P. P. Yang and J. Lin, Adv. Funct. Mater., 2007, 17, 1459.

26 B. Liu, J. Zhang, X. F. Wang, G. Chen, D. Chen, C. W. Zhou and G. Z. Shen, Nano Lett. 2012, 12, 3005.

27 F. J. Sun, X. G. Li, L. P. Liu and J. Wang, Sensor. Actuat. B Chem., 2013, 184, 2013, 220.

28 K. Karthikeyan, D. Kalpana and N. G. Renganathan, Ionics, 2009, 15, 107.

29 M. Davis, C. Gumeci, B. Black, C. Korzeniewski and L. Hope-Weeks, RSC Adv., 2012, 2, 2061.

30 B. Liu, B. Y. Liu, Q. F. Wang, X. F. Wang, Q. Y. Xiang, D. Chen and G. Z. Shen, ACS Appl. Mater. Interfaces, 2013, 5, 10011.

31 L. Cao, F. Xu, Y. Y. Liang and H. L. Li, Adv. Mater., 2004,16, 1853.

32 K. C. Liu and M. A. Anderson, J. Electrochem. Soc., 1994,143,124.

33 X. Y. Chen, C. Chen, Z. J. Zhang and D. H. Xie, J. Mater. Chem. A, 2013, 1,

10903.

34 Z. H. Wang, Q. Sha, F. W. Zhang, J. Pu and W. Zhang, CrystEngComm, 2013, 15, 5928.

35 S. Vijayanand, P. A. Joy, H. S. Potdar, D. Patil and P. Patil, Sens. Actuators, B, 2011, 152, 121.

36 I. Grohmann, B. Peplinski and W. Unger, Surf. Interface Anal., 1992, 19, 591.

37 M. Toupin, T. Brousse and D. Belanger, Chem. Mater., 2002, 14, 3946.

38 Z. Q. Niu, P. S. Luan, Q. Shao, H. B. Dong, J. Z. Li, J. Chen, D. Zhao, L. Cai, W. Y. Zhou, X. D. Chen and S. S. Xie, Energy Environ. Sci., 2012, 5, 8726.

39 F, Zhang, C. Z. Yuan, X. J. Lu, L. J. Zhang, Q. Che and X.G. Zhang, J. Power Sources, 2012, 203, 250.

40 M. J. Deng, F. L. Huang, I. W. Sun, W. T. Tsai and J. K. Chang, Nanotechnology, 2009, 20, 175602.

Figure captions

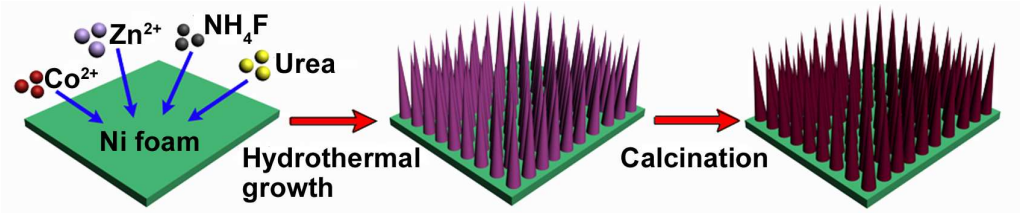

Fig.1 Schematic image of the formation processes of the $ZnCo_2O_4$ nanowires.

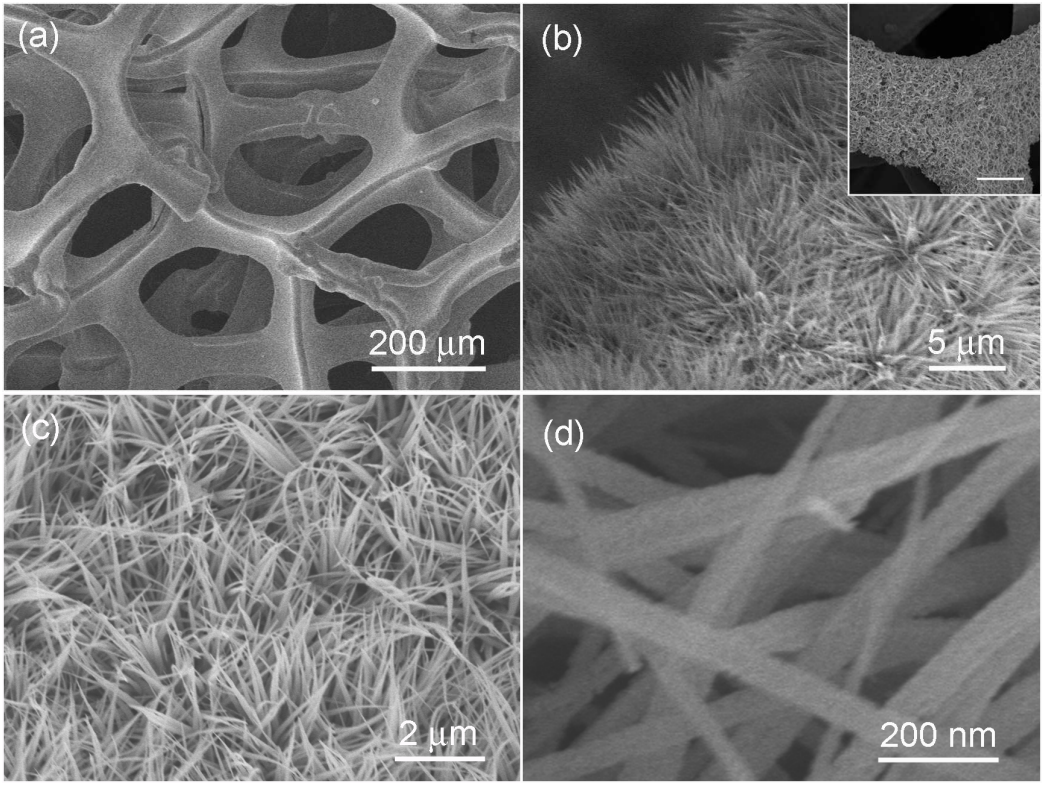

Fig. 2 (a) SEM image of pure nickel foam; (b) SEM image of the precursor on nickel foam, inset show a low-magnified view, scale bar in the inset is 50 μm; (c,d) SEM images of $ZnCo_2O_4$ nanowires on nickel foam with different magnification.

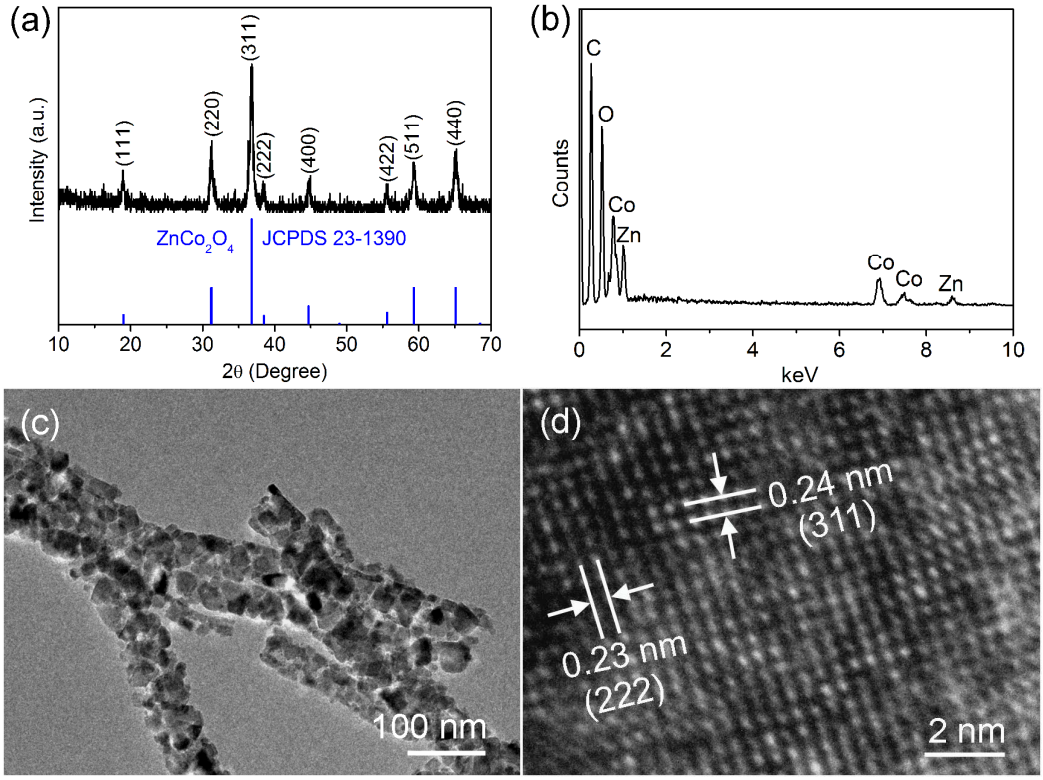

Fig. 3 (a) XRD pattern, (b) EDX spectrum, (c) TEM image, and (d) HRTEM image of $ZnCo_2O_4$ nanowires.

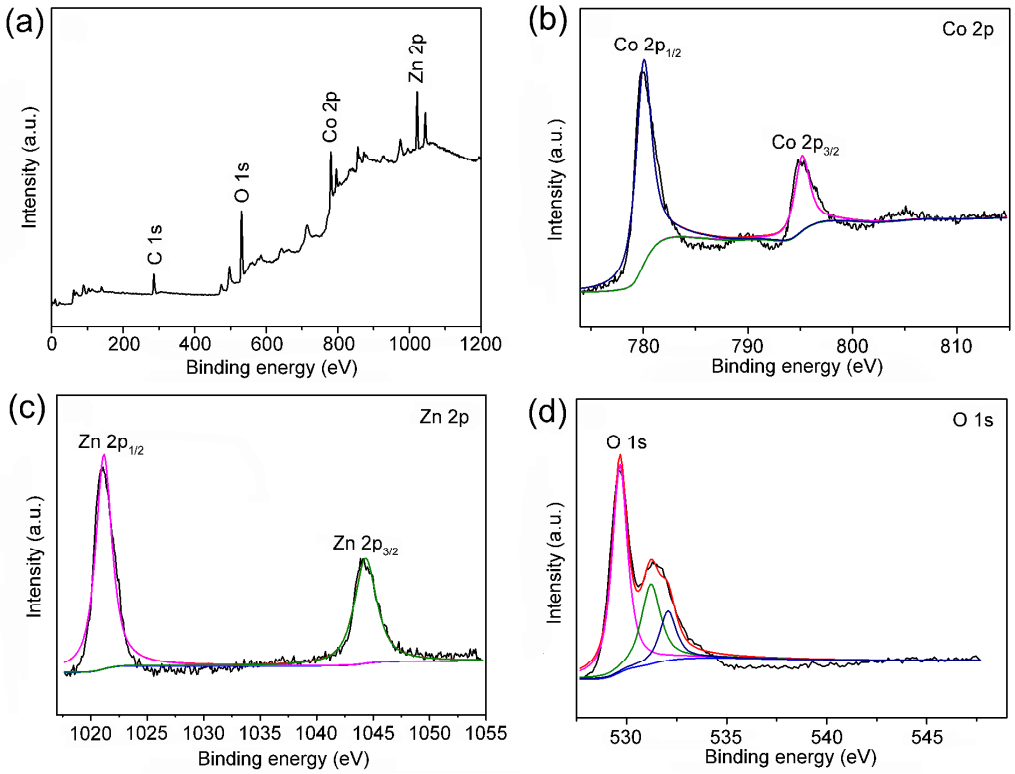

Fig. 4 XPS spectra of $ZnCo_2O_4$ nanowires, (a) survey spectrum, (b) Co 2p, (c) Zn 2p, and (d) O 1s.

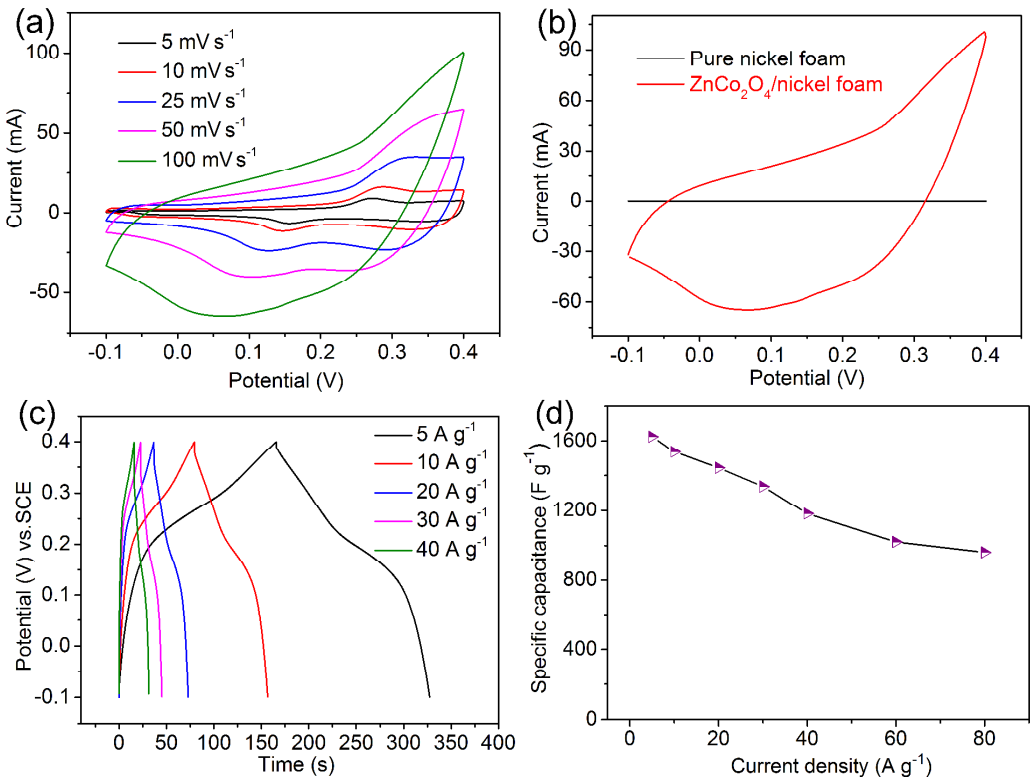

Fig. 5 (a) CV curves of the $ZnCo_2O_4$ nanowire arrays/nickel foam electrode at different scan rates; (b) Comparative CV curves at 100 mV s^{-1} for $ZnCo_2O_4$ nanowire arrays/nickel foam and pure nickel foam; (c) Charge–discharge curves at a series of current densities for $ZnCo_2O_4$ nanowire arrays/nickel foam electrode; (d) Specific capacitances as a function of the current densities of the $ZnCo_2O_4$ nanowire arrays/nickel foam electrode.

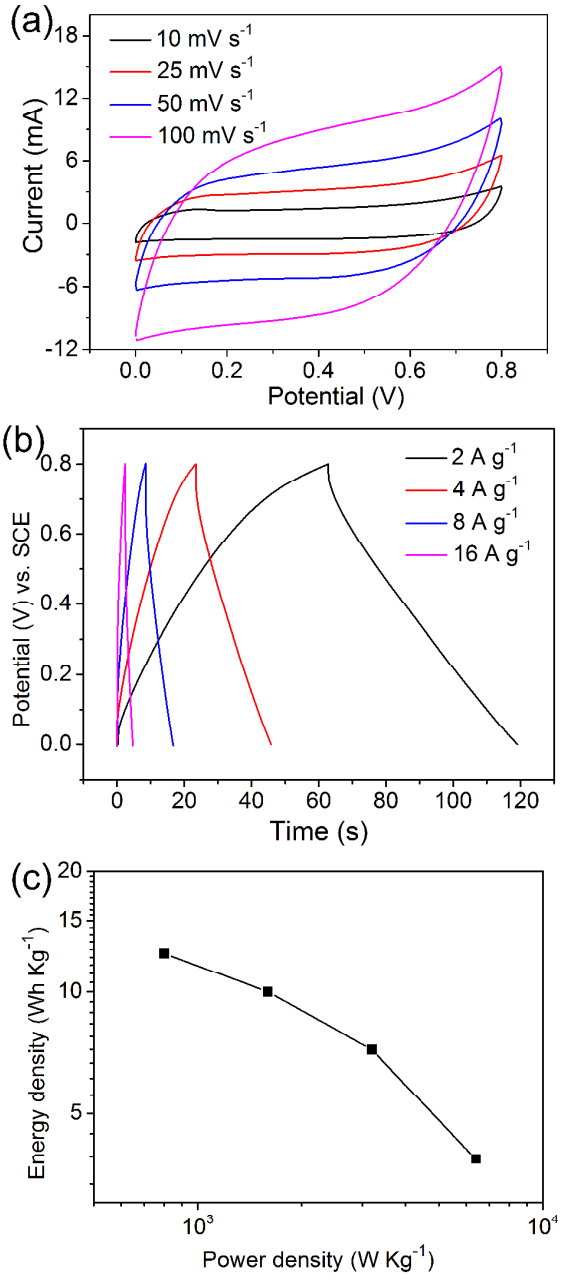

Fig. 6 (a) CV curves of $ZnCo_2O_4$ nanowire arrays/nickel foam electrode at different scan rates in a two electrode system; (b) Galvanostatic charge–discharge curves measured at various current densities in the two electrode system. (c) Ragone plot showing energy density *vs*. power density.

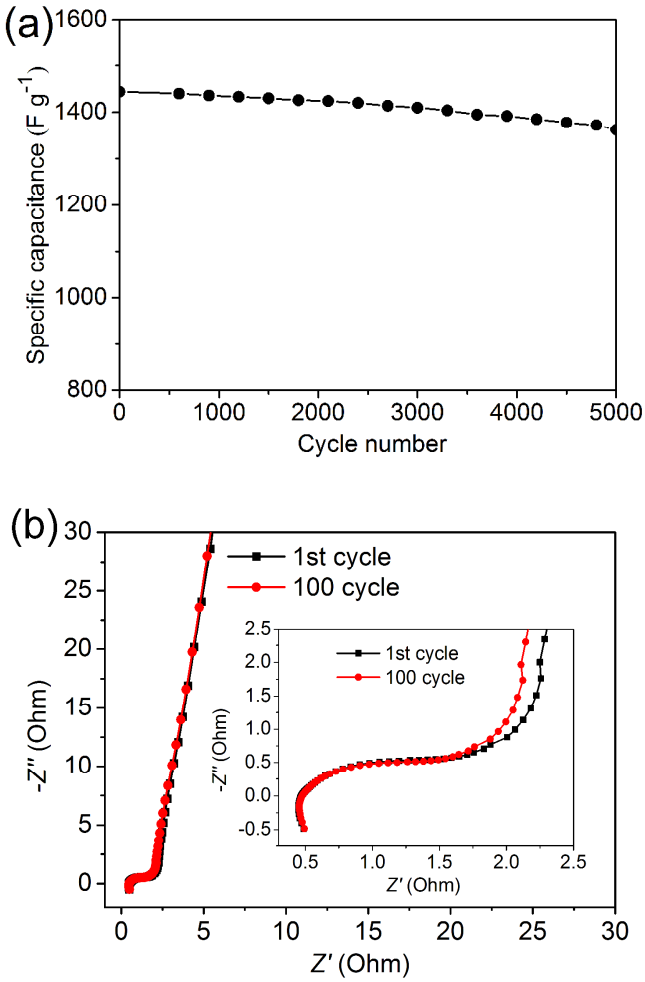

Fig. 7 (a) Cycling performances of $ZnCo_2O_4$ nanowire arrays/nickel foam electrode for 5000 cycles; (b) Nyquist plots of the first and the 100th cycles.

Graphical Abstract

$ZnCo_2O_4$ nanowire arrays on nickel foam as high-peforamnce supercapacitor electrode were synthesized through a hydrothermal and subsequent annealing process.